Supplemental Information

Conformational Dynamics of Light-Harvesting Complex II in a Native Membrane Environment

Fatemeh Azadi-Chegeni, Meaghan E. Ward, Giorgio Perin, Diana Simionato, Tomas Morosinotto, Marc Baldus, and Anjali Pandit

Table S1

Fluorescence lifetime analysis of U-^{13}C-^{15}N Cr LHCII in α-DM and in proteoliposomes.

Sample	A1	τ_1 (ns)	A2	τ_2 (ns)	A3	τ_3 (ns)	τ_{av} (ns)
^{13}C-^{15}N LHCII in α-DM	62%	3.8	18%	1.5	20%	0.1	3.5
^{13}C-^{15}N LHCII proteoliposomes	1%	7.2	65%	0.7	34%	0.3	0.7

Table S2

Assignment of mobile amino-acid residue types detected in the *J*-based INEPT-TOBSY spectrum of LHCII.

Residue type	Cα [ppm]	Cβ [ppm]	Cγ [ppm]	Cδ [ppm]	Cε [ppm]
Ala	52.4	19.3			
	53.3	18.9			
	53.8	19.8			
Thr	61.9	69.7	21.5		
	63.2	68.6	22.2		
		71.1	22.8		
Ser	58.2	63.8			
	59.3	62.9			
	60.0	64.7			
Phe	58.8	39.1	137.5	131.9	
Ile	62.4	38.6	17.4	13.3	
Lys	57.2	32.7	24.2		41.4
Val	63.2	31.9	20.6	19.3	
Glu	57.3	29.7			
Asn	53.1	38.9			
Leu	56.1	42.5			
Pro	63.8	31.5	26.4	48.9	
			27.4	50.8	
			26.9	49.5	
Asp/Leu	54.2	41.0			

Table S3

Assignment of Chlorophyll tail ^{13}C resonance signals detected in the *J*-based INEPT-TOBSY spectrum of LHCII.

Carbon atom	Chemical shift (ppm)	
	Chl i [ppm]	Chl ii[ppm]
P1	60.8	62.9
P2	121.6	126.1
P3	140.8	143.5
P3a	18.4	18.4
P4	42.5	42.1

Table S4

Assignment of ^{13}C lipid resonance signals detected in the *J*-based INEPT-TOBSY spectrum of LHCII and in the spectrum of thylakoid membranes.

Carbon atom	Chemical shift (ppm)	
	MGDG	DGDG
C1	105.9	101
C2	75.4	74.3
C3	73.4	-
C4	68.9	77.7
C5	-	71.1
C6	65	54.6
C7	-	-
C8	130.2	130.2
C9	132.1	132.1
C10	29.6	29.6
C11	27.9	27.9
C12	130.7	130.7
C13	-	-
C14	27.8	27.8
C15	129.6	129.6
C16	133.8	133.8
C17	23.1	23.1
C18	16.66	16.66

Figure S1

LHCII structure and abundancy in thylakoid membranes. A: Protein structure. B: LHCII structure including the pigments, with Chl *a* in green, Chl *b* in blue, lutein in red and neoxanthin in purple and violaxanthin in yellow. C: top view of trimeric LHCII. D: Sucrose gradient of *Cr* thylakoid membranes after solubilizing with 0.6% α-DM, showing the fraction of trimeric LHCII. E: SDS page gel image of the *Cr* thylakoid membranes and of isolated LHCII.
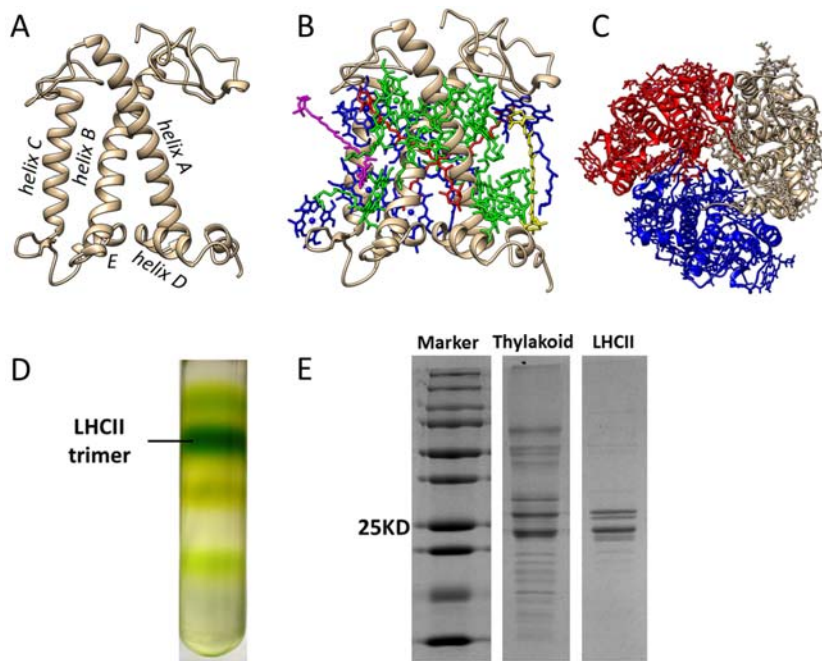
Figure S2

A: Example of thylakoid extraction using a layered sucrose gradient. a. eye spot containing β-carotenes; b. thylakoid membranes; c. cell walls and unbroken cell material. Band b was extracted with a syringe and contained the purified thylakoid fraction.

B: Absorption spectra of ^{13}C *Cr* thylakoid membranes. The Q_y absorbance bands of Chl*a* and *b* at are distinguished at 672 and 650 nm respectively, and carotenoids and Chl higher-energy states contribute to the spectrum in the region between 400 and 500 nm.
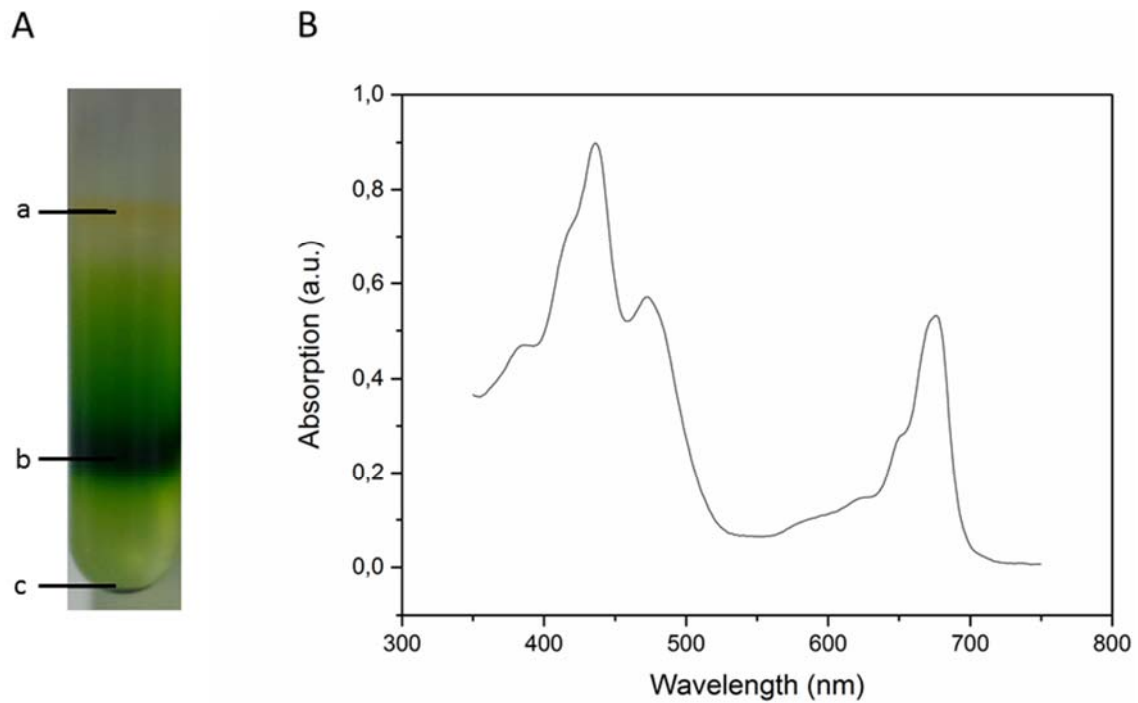
Figure S3

77K fluorescence spectrum of LHCII in α-DM (black) and of LHCII proteoliposomes (red). The band at 700 nm is a signature of LHCII aggregation in the proteoliposomes.
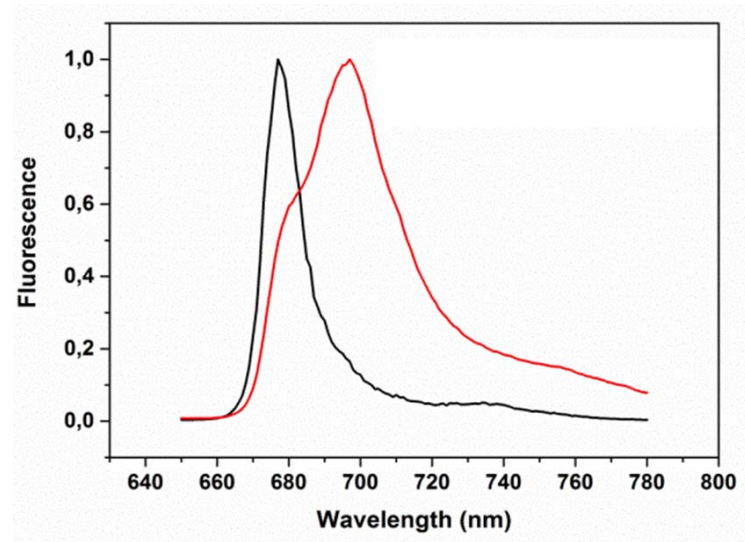
Figure S4

Time-resolved fluorescence decay of LHCII in α-DM (green) and of LHCII proteoliposomes (black). Dotted lines in blue and red are exponential fit curves using three components.
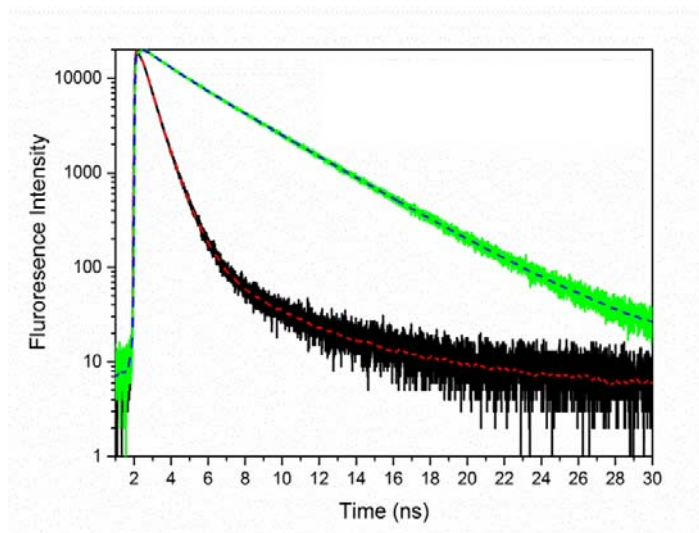
Figure S5

CP-PARIS ^{13}C-^{13}C spectrum of LHCII proteoliposomes, aliphatic region. The spectrum was collected with a mixing time of 30 ms at 17 kHz MAS at a set temperature of -18 ℃.
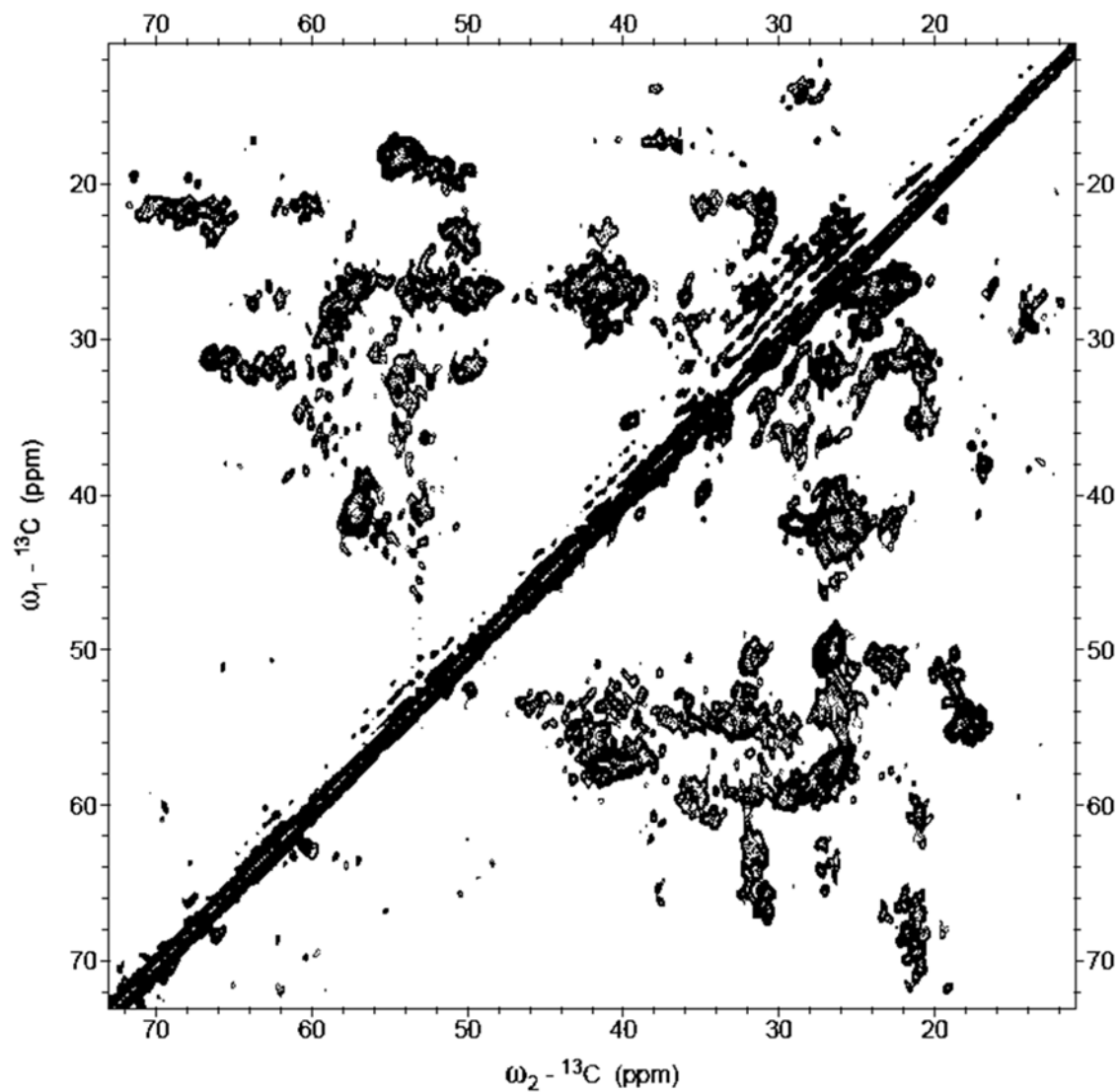
Figure S6

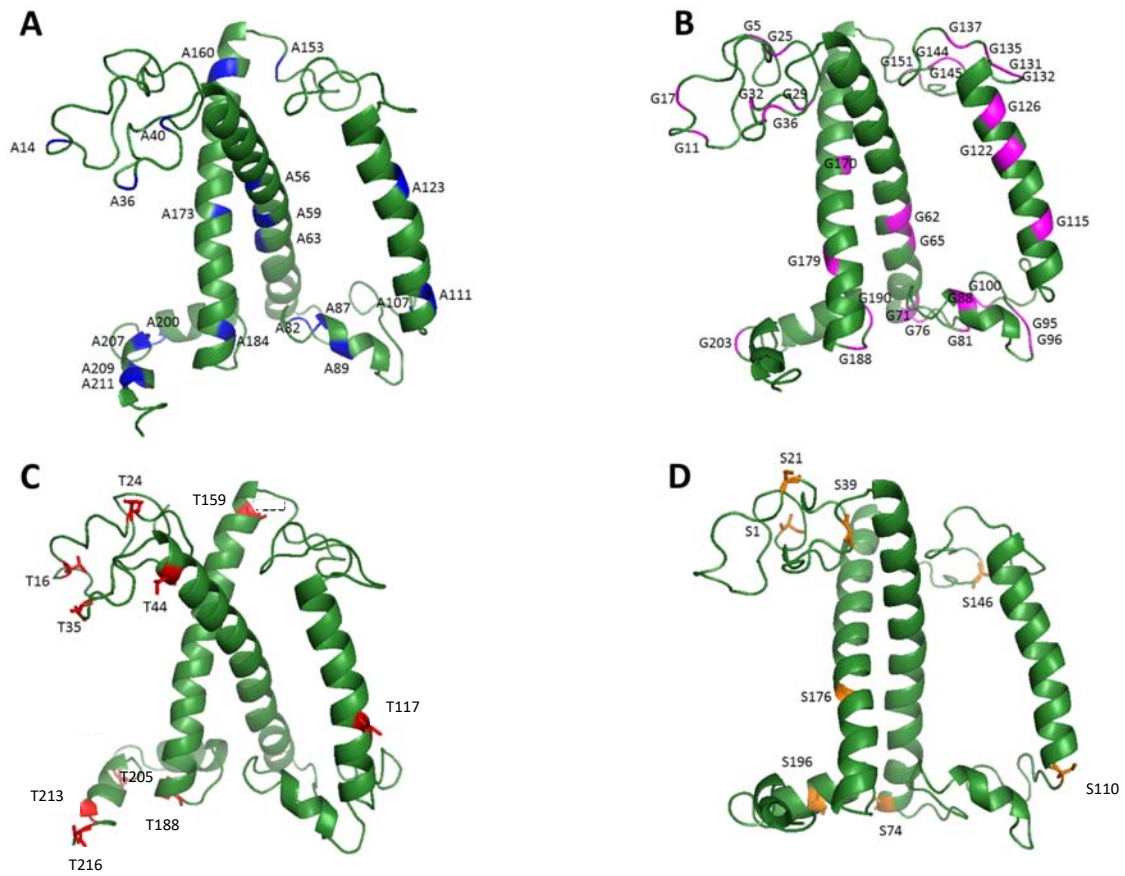Structure of Lhcbm1, highlighting Ala (A), Gly (B), Thr (C) and Ser (D) residues.

Figure S7

Helix and coil percentages according to the NMR spectrum, *Cr* LHCII homology model based on Lhcbm1 (model1), Lhcbm2/7 (model2) or Lhcbm3 (model3) and according to the full amino acid sequence of Lhcbm3 (sequence3). The Lhcbm1 model lacks the N-terminal amino acids that are present in the sequence. The structural model for Lhcbm2 contains the full protein sequence as this polypeptide has no N tail.
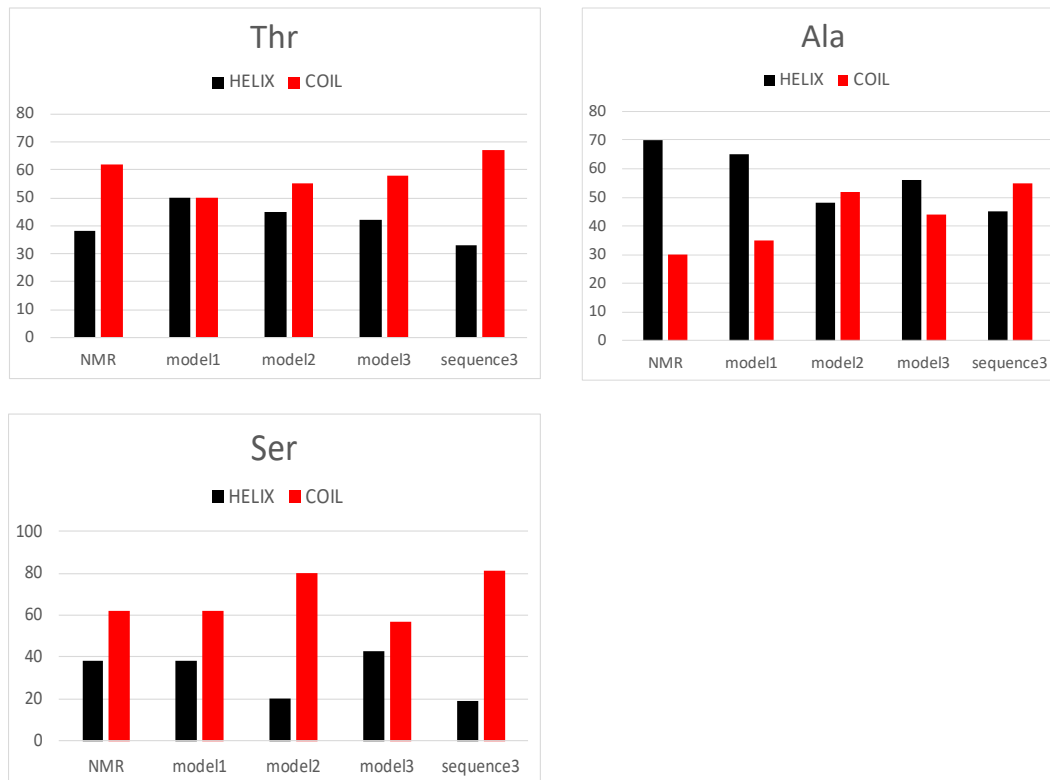
Figure S8

Comparison of 1D-^{13}C CP-MAS and direct excitation (DP)-MAS spectra. Overlaid ^{13}C CP (black) and direct excitation (DP, green) spectra of thylakoid membranes containing LHCII (A) and of LHCII proteoliposomes (B). The spectra were collected with 512 scans, 2 second of recycle delay, 80 ms acquisition time at 14 kHz. For CP-MAS experiments, the mixing time was set to 1 millisecond. The set temperature was -3 °C.
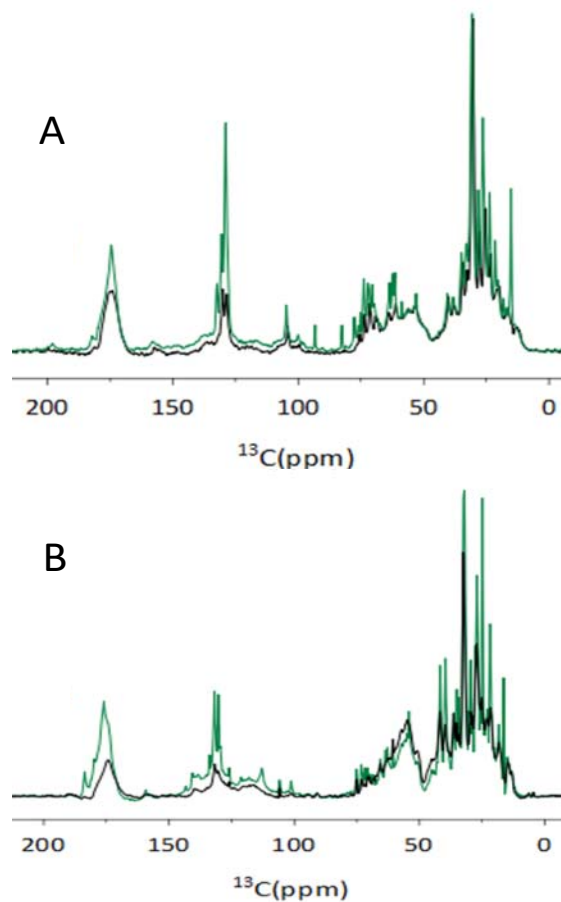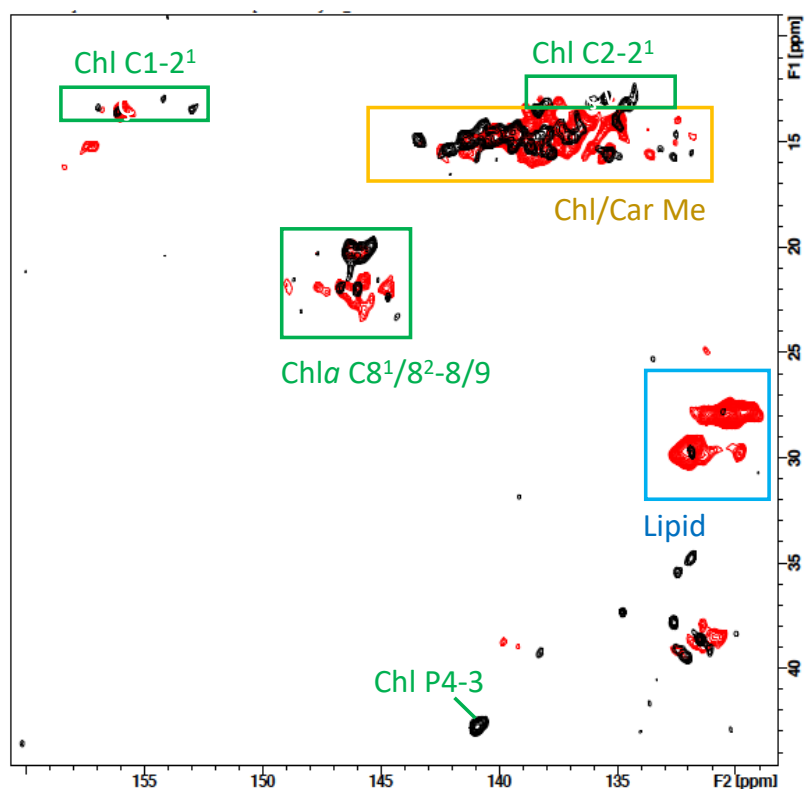
Figure S9

^{13}C-^{13}C CP-PARIS spectrum of LHCII proteoliposomes (red) and of thylakoid membranes containing LHCII (black). Spectra were collected with a mixing time of 30 ms at 17 kHz MAS at a set temperature of -18 °C.

Below: Aromatic region showing correlation signals of Chls and carotenoids (Car).

Next page: Selective 1D slices of the ^{13}C-^{13}C CP-PARIS spectrum of LHCII proteoliposomes (red) and of thylakoid membranes containing LHCII (black) with Ala, Ser and Thr peaks in helix and coil regions.
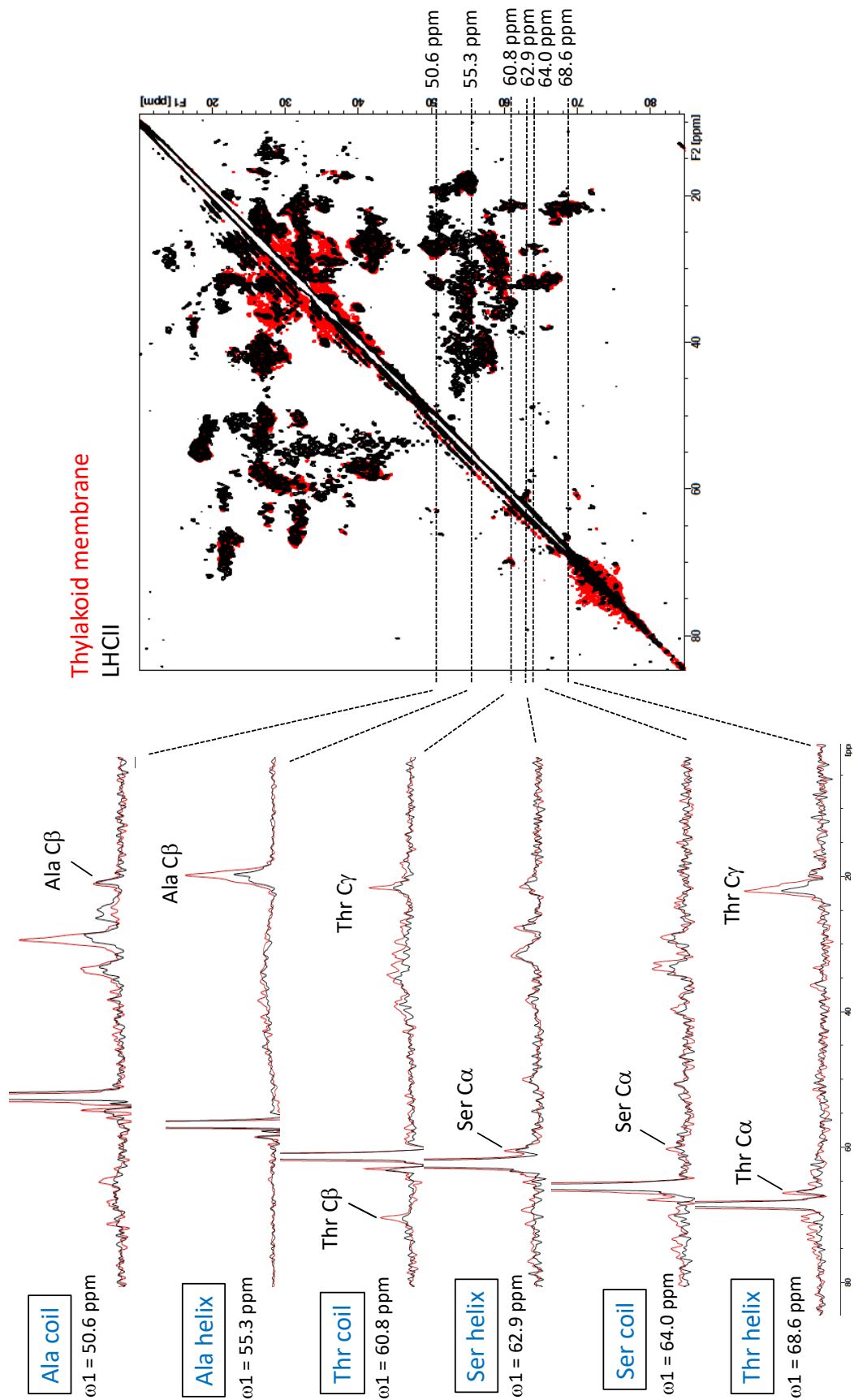
Thylakoid membrane
LHCII

50.6 ppm
55.3 ppm
60.8 ppm
62.9 ppm
64.0 ppm
68.6 ppm

Ala Cβ

Ala Cβ

Thr Cγ

Ser Cα

Thr Cβ

Ser Cα

Thr Cγ

Thr Cα

Ala coil
ω1 = 50.6 ppm

Ala helix
ω1 = 55.3 ppm

Thr coil
ω1 = 60.8 ppm

Ser helix
ω1 = 62.9 ppm

Ser coil
ω1 = 64.0 ppm

Thr helix
ω1 = 68.6 ppm

Figure S10

CP-PARIS ^{13}C-^{13}C spectrum of LHCII proteoliposomes (black) overlaid with SHIFTX2-generated protein correlations prediction of Lhcbm1 (cyan) and Lhcbm2 (orange). The spectrum was collected with a mixing time of 30 ms at 17 kHz MAS at a set temperature of -18 °C.
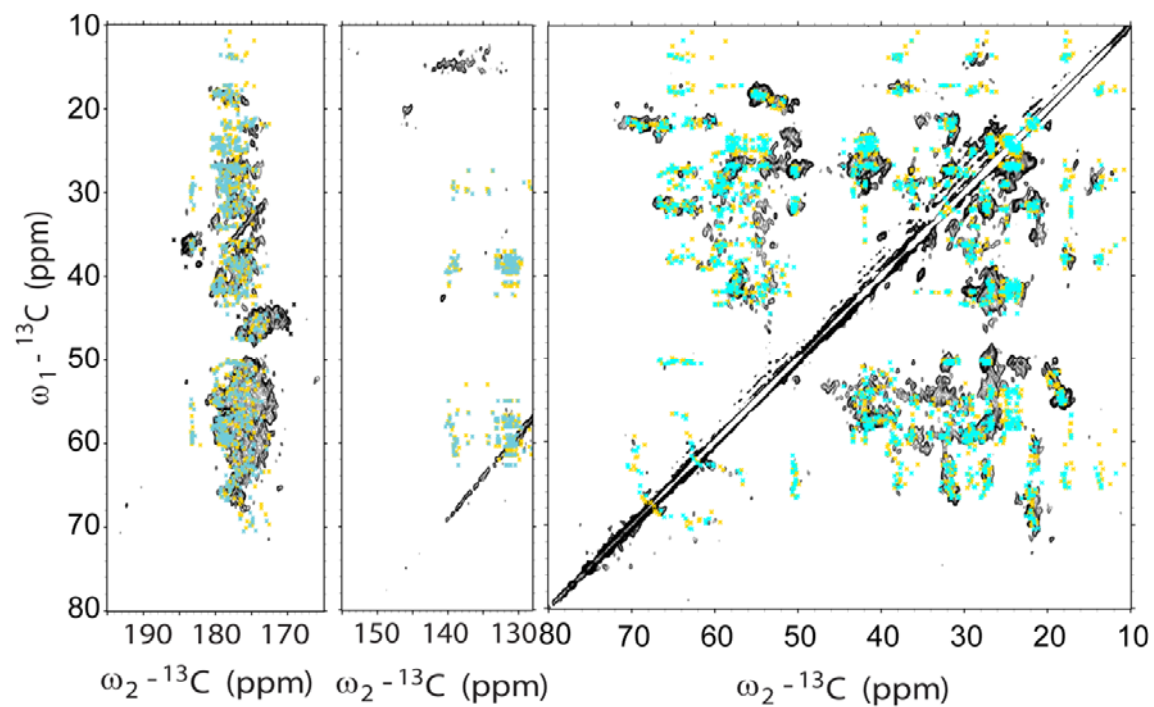
Figure S11

NCA ^{15}N-^{13}C spectrum of LHCII proteoliposomes (black) overlaid with predicted correlations of Lhcbm1 (red dots) and Lhcbm2 (green dots). The NCA spectrum was collected at 14 kHz MAS frequency at -18 °C, using a mixing time of 800 μs ^{1}H-^{15}N CP step, 4.2 ms for ^{15}N-^{13}C and the number of scans was set to 704. Significant deviations between predicted and experimentally observed cross peaks are observed for Val106, Ile111, Thr188 and Thr213 in Lhcbm1, and in Gly20, Ile114 and Thr216 in Lhcbm2.
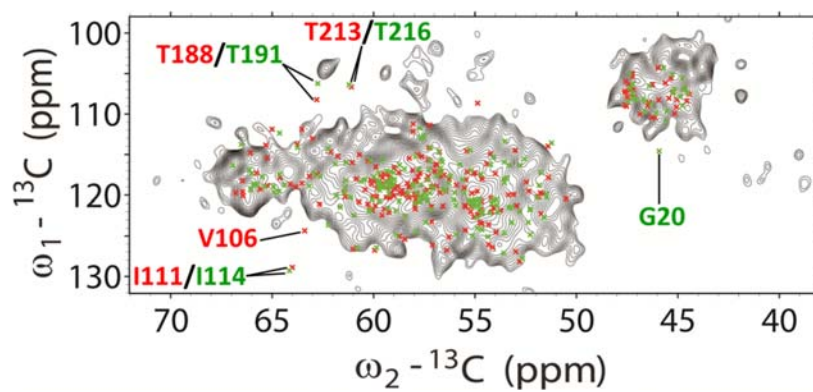
Figure S12

A-D: Overlay of the INEPT-TOBSY spectrum of LHCII proteoliposomes (black) and of thylakoid membranes containing LHCII (red). Protein assignments are indicated in black, Chl assignments in green and lipid assignments in blue. Spectra were collected at -3 °C. E: Chemical structure of MGDG, highlighting the lipid atom types that could be distinguished in the INEPT-TOBSY spectrum.
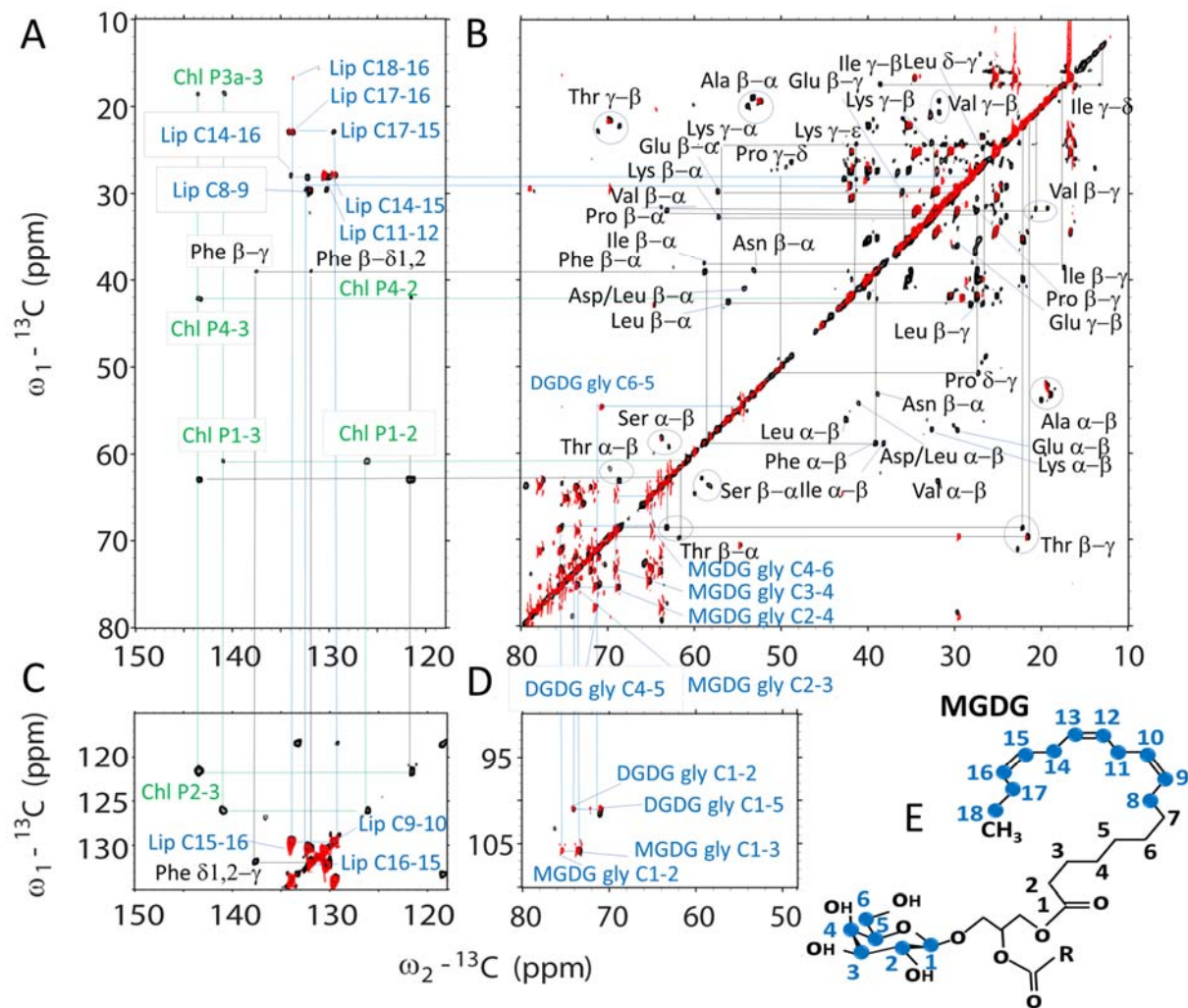
Figure S13

Overlaid ^{13}C-^{13}C PARIS (black) and ^{13}C-^{13}C INEPT-TOBSY (blue) spectra of LHCII proteoliposomes. The insets show the Ala, Ser and Thr signals. The CP-PARIS spectrum was recorded at a set temperature of 255 K and the INEPT-TOBSY spectrum at a set temperature of 270 K. One Ser and two Ala peaks overlap in the two spectra.
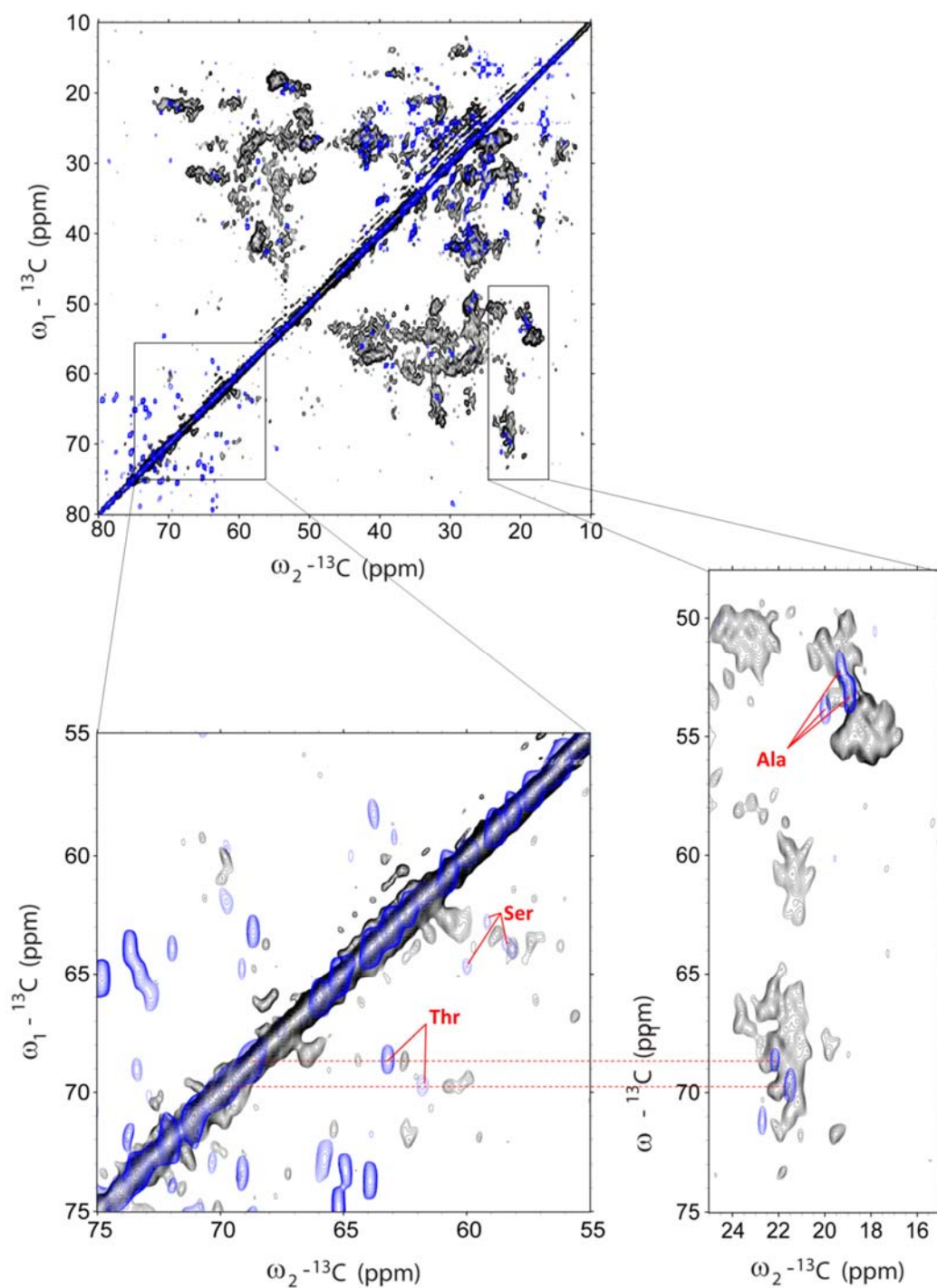
Figure S14

Overlaid INEPT-TOBSY (red) and DP-PARIS (blue) spectrum showing correlations of Chl phytol (P) carbon atoms. The spectra were collected at -3 °C and 14 kHz MAS. For the TOBSY spectrum, a mixing time of 6 ms was applied.
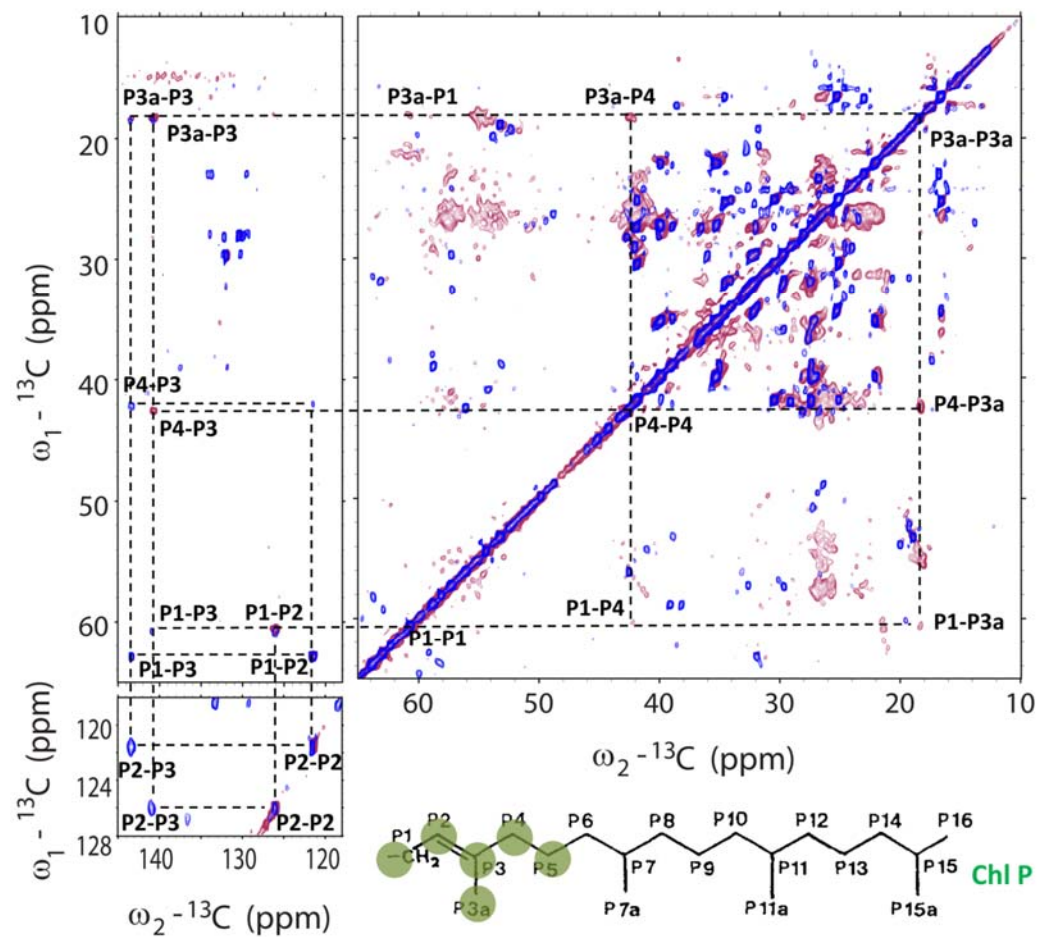
Figure S15

NMR comparison of structure-predicted and experimental NMR chemical shift correlations. A-D: ^{13}C-^{13}C CP-PARIS spectrum of thylakoid membranes containing LHCII (red) with the LHCII proteoliposome spectrum (black) overlaid. The insets show Ala (B), Thr (C) and Ser (D) spectral regions overlaid with chemical-shift predictions of Lhcbm1 (cyan crosses) and Lhcbm2 (black crosses). Predicted shifts that significantly deviate from experimental correlations are highlighted in yellow.
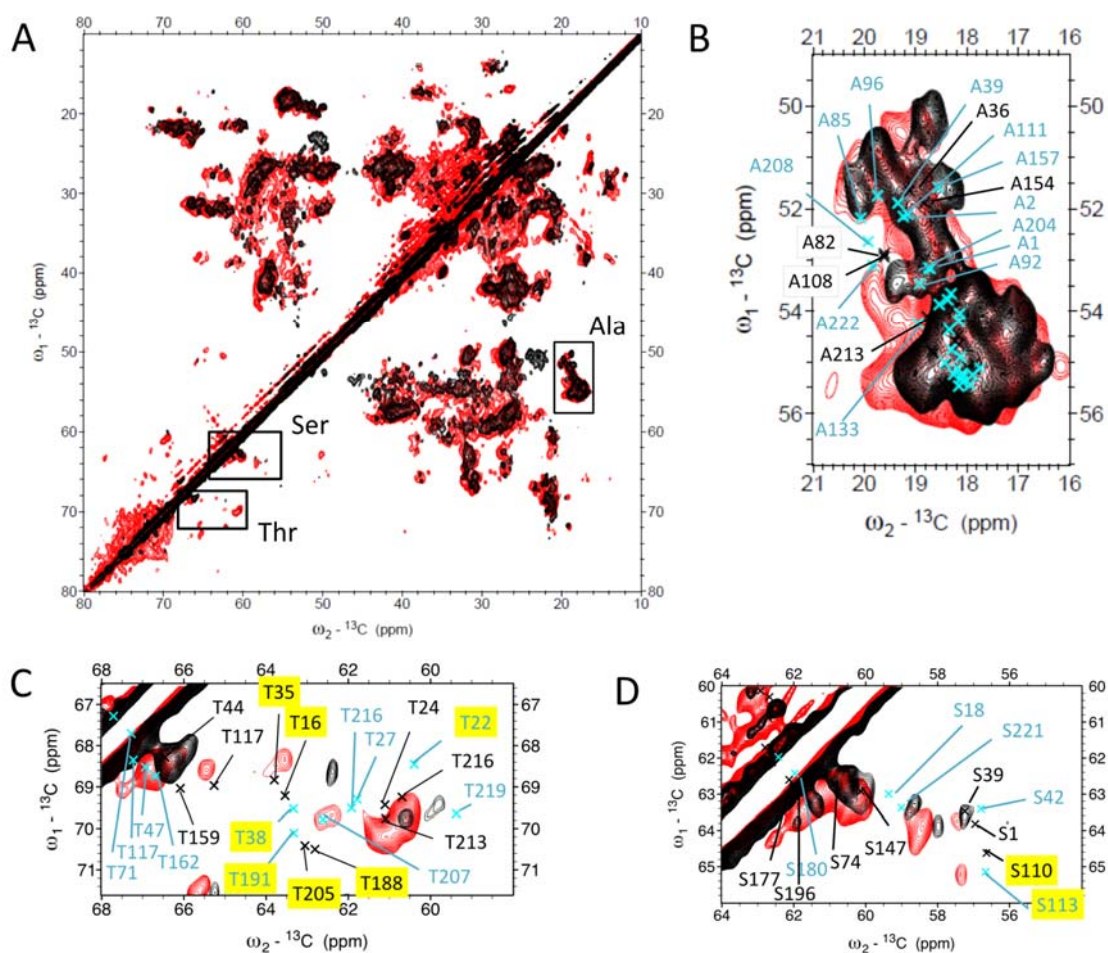
References

1.   Krishna K. Niyogi OB, and Arthur R. Grossman (1997) Chlamydomonas Xanthophyll Cycle Mutants ldentified by Video Imaging of Chlorophyll Fluorescence Quenching *The Plat Cell* 9:1369-1380.

2.   Laemmli UK (1970) Cleavage of Structural Proteins during the Assembly of the Head of Bacteriophage T4. *Nature* 227:680-685.

3.   A. Pinest MGG, and J. S. Waugh (1973) Proton-enhanced NMR of dilute spins in solids. *Journal of Chemicla Physiscs* 69(2):569-590.

4.   Hartmann SR & Hahn EL (1962) Nuclear Double Resonance in the Rotating Frame. *Physical Review* 128(5):2042-2053.

5.   Baldus M, Petkova AT, Herzfeld J, & Griffin RG (1998) Cross polarization in the tilted frame: assignment and spectral simplification in heteronuclear spin systems. *Molecular Physics* 95(6):1197-1207.

6.   B. M. Fung (2000) An Improved Broadband Decoupling Sequence for Liquid Crystals and Solids. *Journal of Magnetic Resonance* 142:97-101.

7.   Weingarth M, Demco DE, Bodenhausen G, & Tekely P (2009) Improved magnetization transfer in solid-state NMR with fast magic angle spinning. *Chemical Physics Letters* 469(4-6):342-348.

8.   Baldus M (2002) Correlation Experiments for Assignment and Structure Elucidation of Immobilized Polypeptides Under Magic Angle Spinning. *Prog. Nucl. Magn. Reson. Spectr* 1-47(1-2).

9.   Baldus M & Meier BH (1996) Total Correlation Spectroscopy in the Solid State. The Use of Scalar Couplings to Determine the Through-Bond Connectivity. *Journal of Magnetic Resonance, Series A* 121(1):65-69.

10.   Gareth A. Morris aRF (1979) Enhancement of nuclear magnetic resonance signals by polarization transfer. *J. Am. Chem. Soc* 101(3):760–762.

11.   T. D. Goddard and D. G. Kneller, SPARKY 3, *University of California, San Francisco*

12.   Arnold K, Bordoli L, Kopp J, & Schwede T (2006) The SWISS-MODEL workspace: a web-based environment for protein structure homology modelling. *Bioinformatics* 22(2):195-201.

13.   Natali A & Croce R (2015) Characterization of the major light-harvesting complexes (LHCBM) of the green alga Chlamydomonas reinhardtii. *PLoS One* 10(2):e0119211.

14.   Han B, Wishart DS, Liu Y, & Ginzinger SW (2011) SHIFTX2: significantly improved protein chemical shift prediction. *J Biomol NMR* 50:43-57.

15.   Gradmann S, *et al.* (2012) Rapid prediction of multi-dimensional NMR data sets. *J Biomol NMR* 54:377-387.